Journal of Engineering Science and Technology
Vol. 14, No. 5 (2019) 2731 - 2745

ELECTROMAGNETIC SIGNATURE STUDY OF A CLOSED LOOP SPEED CONTROLLED THREE-PHASE INDUCTION MOTOR UNDER BROKEN ROTOR BAR FAULT USING FINITE ELEMENT METHOD

PRAVEEN KUMAR N.*, ISHA T. B.

Department of Electrical and Electronics Engineering, Amrita School of Engineering, Coimbatore, Amrita Vishwa Vidyapeetham, India
*Corresponding Author: n_praveenkumar@cb.amrita.edu

Abstract

This paper investigates an electromagnetic signature study of a closed loop speed controlled three phase Induction Motor (IM) fed from a PWM (pulse width modulated) inverter under single broken bar rotor fault using Finite Element Method (FEM) analysis co-simulated with MATLAB Simulink environment. As the electromagnetic field signatures of the IM contains the entire information in relation to the position of stator, rotor and mechanical parts of the machine, a continuous monitoring of airgap electromagnetic fields can be used for the identification of rotor broken bar fault in IM. In this direction, IM with a healthy and rotor broken bar model is created using ANSYS Maxwell Finite Element Analysis (FEA) tool and various electromagnetic field parameters like flux lines, flux density and radial airgap flux density distribution are studied. In addition, a study is done on the voltage induced in the end connection of the squirrel cage rotor for healthy and broken bar IM. The power electronic converter with its control scheme is modeled in MATLAB Simulink and co-simulated with ANSYS Simplorer and ANSYS Maxwell to integrate all the components in one common simulation platform environment for exact design and analysis for realistic simulation.

Keywords: Broken rotor bar, Closed loop speed control, Electromagnetic fields, Finite element method, Radial airgap flux density.

1. Introduction

Three-phase induction motors (IM's) are universally used motors in all the industries, which constitutes nearly 80% of the industrial motors due to its roughness and versatility. In the current scenario, for variable speed applications, most of the IM's are operated from pulse width modulated (PWM) inverter drives, resulting in huge energy and cost saving for the industries. Even though IM's are very reliable, it is subjected to various types of faults either in the machine or in the inverter when used for adjustable speed applications. One of the important faults, which constitute nearly 7% of the entire IM breakdown, is rotor bar fault [1]. The root cause of rotor broken bar in IM is due to various stresses occurring on the machine namely thermal, electromagnetic, residual, mechanical, dynamic and environmental due to wide variety of reasons. In addition to the above stresses, when the machine is operated from PWM inverter, which is the source for inherent noise, the stator winding is subjected to abrupt voltage transitions accompanied by switching action of power electronic switches.

Extensive research is carried out since 1980's for diagnosing the broken rotor bar fault when IM is fed from mains. The most popular technique which is still widely used in industries for finding rotor bar fault is the MCSA (Motor Current Signature Analysis) based on the signature of stator current in the FFT spectrum. When a bar breakage occurs in an IM, in addition to the forward magnetic field an inverse component of magnetic field will be produced which will induce oscillations in torque and speed of IM. The torque oscillations will be reflected in the stator current at the frequencies $(1\pm2s)f$ where s is per unit slip and f is line frequency. However, MCSA technique is ineffective when the machine is operated under a load torque that is oscillating and also when operated at variable speeds. The load or coupling also produces components at the same frequencies, which makes the fault difficult to detect. Several other indicative methods can be observed in the literature [1] when the machine fed from mains is operated at constant load torque and at constant speed. Not too many researchers have established approaches for rotor faults under varying load torque conditions [2].

Recently in most of the industries due to widespread use of automation, speed of the PWM inverter fed IM is controlled automatically by employing various closed loop control approaches differing from basic closed loop *v/f* control to complex behaviour drives based on DTC, FOC or other form of vector control techniques. The diagnostic techniques developed for mains fed IM are not capable in closed loop applications because the control strategy will tend to preserve normal operation of the drive even when a fault occurs, masking the fault indicators [1]. Also, real-time monitoring approaches can flounder if the frequency changes frequently for variable speed operation. The most simple and widely employed method in industries for controlling the speed of inverter fed IM under oscillating load conditions is the closed loop *v/f* control. Very few research works are spotted in literature on diagnostic procedures for rotor faults in inverter fed IM operating under closed loop *v/f* control strategy.

Although techniques based on lumped parameter equivalent circuit model and winding function method are used to diagnose the rotor fault, they ignore various parameters like spatial harmonics of the airgap flux, magnetic saturation, non-linear behaviour of magnetic material etc. Therefore, the above said analytical methods cannot show the real functioning of the IM under faulty condition. In order to include the above mentioned parameters, FEM is used which is based on electromagnetic field analysis that also incorporates actual representation of

stator windings and rotor bars, magnetic circuit geometry and existing slots around airgap.

A flux measurement procedure based on emf induced in a search coil wound on the stator tooth is used to detect rotor bar fault in mains fed and inverter driven IM based on FEM [3]. This is an invasive method since it requires a search coil to be wound on the stator tooth. According to Gyftakis et al. [4], electromagnetic torque spectrum around the frequency range of 300 Hz is used for detecting broken bar fault in mains fed IM using FEM. A technique based on airgap torque profile data obtained from FEM and processed in concurrence with a Bayesian classifier is used to determine the rotor bar fault in mains fed IM [5]. Drawback of this method is the offline training required for IM with datasets generated from FEM. An offline inspection technique for closed loop inverter fed IM based on the variation of impedance pattern under standstill condition is used as an index to detect rotor bar fault [6]. Authors verified the results by using FEA simulation results, but it does not provide continuous monitoring.

Radial airgap flux density is analysed for phase short-circuit fault of open loop PWM inverter fed IM using FEM [7]. The electromagnetic field analysis based on radial airgap flux density is done for broken rotor bar fault of open loop Sine PWM inverter fed IM using FEA [8]. Bensalem and Abdelkrim [9] mentioned that the modelling and simulation of IM is based on ANSYS Maxwell FEA, in which, it co-simulated with ANSYS Simplorer and with MATLAB Simulink for implementing open loop *v/f* controlled PWM inverter for phase short-circuit fault and analytical parameters like stator voltage, current and torque are analysed. As mentioned by Godot et al. [10], closed loop speed controlled IM's are popularly used in many industrial applications and the control strategy affects the performance and cause degradation in traditional fault diagnosis methods. Closed loop control changes the nature of supply parameters and provides unreliable results unless the diagnosis methods consider its impacts [11].

Based on studies by Nemec et al. [12], arithmetic mean duty cycle of the modulated inverter output voltage is used for detecting broken bar fault in closed loop controlled IM, but detecting the fault at the incipient stage is not possible as this method is influenced by control technique. Abu-Elhaija et al. [13] proposed that the disturbance created by the closed loop control strategy on the inverter output voltage for diagnosing broken rotor bar fault. Hou et al. [14] reported that the influence of closed loop control on the sideband components of stator current is neglected for detecting broken bar fault in *Y* connected IM.

Hou et al. [15] have used a fault severity factor to detect one and two broken bars in a closed loop controlled IM, which shows large difference between calculated and practical values due to negligence of parameters like magnetic saturation, spatial harmonics and inter-bar currents. In this framework, the proposed method includes all the above said factors in FEM, can be used to analyse broken rotor bar fault at the incipient stage in a closed loop speed controlled IM.

In this paper, an electromagnetic signature study is conducted on a 3 φ squirrel cage IM fed from closed loop speed controlled PWM inverter under broken rotor bar fault condition using FEM. Various electromagnetic parameters like flux lines and flux density distribution, radial airgap flux density and voltage induced in the end-ring of rotor are analysed. ANSYS Maxwell FEA tool is used for modelling of IM co-simulated with ANSYS Simplorer for loading the IM and ANSYS Simplorer

co-simulated with MATLAB Simulink for modelling sine PWM inverter and implementing closed loop *v/f* control strategy. It is also intended to integrate various environments like Maxwell, Simplorer and Simulink in one collective platform, for accurate design and analysis for realistic simulation.

The paper is formulated as follows: Section 2 supports the analytical framework, followed by electromagnetic field investigation of broken bar motor in Section 3. The analysis on airgap flux density and end-ring induced voltage of faulty motor is done in Section 4 accompanied by concluding remarks in Section 5.

2. Analytical Background

According to Boldea and Nasar [16], the stator MMF of IM can be written as,

$$F_1(\theta,t) = \sum_{v=6k\pm1}^{\infty} F_{1mv} Cos(v\theta_e \pm \omega_1 t) \tag{1}$$

where F_{1mv} is the stator amplitude fundamental MMF, v is the stator MMF spatial harmonic, k is an integer, ω_1 is the stator frequency (angular) and θ is the geometrical angle given by,

$$\theta = \frac{\pi x}{p_1 \tau} \tag{2}$$

and $\theta_e = p_1\theta$ where x is the co-ordinate along stator bore periphery, p_1 is the pole pair numbers and τ is spatial half-period of MMF ideal wave. The rotor MMF is given by,

$$F_2(\theta,t) = \sum_{\mu=1}^{\infty} F_{2m\mu} Cos(\mu\theta_e \pm \omega_1 t - \varphi_\mu) \tag{3}$$

where $F_{2m\mu}$ is the amplitude of rotor fundamental MMF, φ_μ is the reference angle between stator $F_1(\theta, t)$ and rotor $F_2(\theta, t)$ fundamental MMF's and μ is the rotor MMF spatial harmonic given by,

$$\mu = \frac{kN_r}{p_1} \pm 1 \tag{4}$$

where N_r is the rotor slot number. The airgap permeance per unit area can be written as sum of mean permeance, harmonics of permeance due to stator and rotor slots and reciprocal effect of stator and rotor [16],

$$\Lambda(\theta,t) = \frac{\mu_o}{\delta_o K_c} + \sum_{k=1}^{\infty} \Lambda_{1,k} Cos(kN_s\theta) + \sum_{\ell=1}^{\infty} \Lambda_{2,\ell} Cos[\ell N_r(\theta - \omega_2 t)] + \sum_{k=1}^{\infty}\sum_{\ell=1}^{\infty} \Lambda_{1,2,k\pm\ell} Cos[(kN_s \pm \ell N_r)\theta - \ell N_r \omega_2 t] \tag{5}$$

where δ_o is the airgap length, K_c is the Carter's coefficient, N_s is the stator slot number, ω_2 is the rotor angular frequency, k and ℓ are integers associated with stator and rotor slots and Λ_1 and Λ_2 are partial permeances. The airgap magnetic flux density of IM can be computed by,

$$B(\theta,t) = \Lambda(\theta,t).F(\theta,t) = \Lambda(\theta,t)[F_1(\theta,t) + F_2(\theta,t)] \tag{6}$$

The effect of magnetic saturation of stator and rotor cores should be considered to analyse the fault precisely at the incipient stage. Boldea and Nasar [16] stated that in FEM, the magnetic saturation of iron core of IM will be taken into account, in addition to the permeance of airgap.

$$\Lambda_{sat}(\theta,t) = -\Lambda_{sat} Cos(2p_1\theta - 2\omega_1 - 2\varphi_s) \quad (7)$$

Therefore, the airgap flux density of IM due to saturation will be,

$$B_{sat}(\theta,t) = \Lambda_{sat}(\theta,t)[F_1(\theta,t) + F_2(\theta,t)] \quad (8)$$

3. Electromagnetic Field Investigation of Rotor Broken Bar Motor

In this section, a study on electromagnetic characteristics of IM under healthy and single broken rotor bar fault condition is done using ANSYS Maxwell FEA tool. Simulation is performed on a 7.5 kW, 3 φ, 4 pole, 380 V IM with 44 rotor slots and 48 stator slots, the details of which are given in Table 1 [17].

Table 1. Three phase induction motor and FEM parameters.

General parameters	
Voltage	380 V
No. of poles	4
Rated speed	1440 rpm
Supply frequency	50 Hz
Power output	7.5 kW
Stator parameters	
Outer diameter	210 mm
Inner diameter	148 mm
Length of the core	250 mm
Steel type	M19_24G
No. of slots	48
Rotor parameters	
Outer diameter	147.3 mm
Inner diameter	48 mm
Airgap	0.35 mm
Steel type	M19_24G
No. of slots	44
FEM Parameters	
Boundary condition	Vector potential
Number of elements	18542
Time step	$2*10^{-4}$ s
Number of time steps	$20*10^3$
Degree of freedom	1.8

The FE model of IM in ANSYS Maxwell is supplied from a PWM inverter controlled by closed loop *v/f* speed control strategy modelled in MATLAB Simulink. A block diagram used for co-simulation between ANSYS Maxwell, ANSYS Simplorer and MATLAB Simulink for FE model of IM, loading arrangements and PWM inverter with closed loop *v/f* speed control strategy is presented in Fig. 1.

With a special function AnsoftSFunction in Simulink, the data is exchanged between Simplorer and Simulink. The three pole voltages (V_a, V_b, V_c) of voltage source inverter (VSI) modeled in Simulink is imported to the IM terminals (Phase A, Phase B, Phase C) in Simplorer and the actual speed data required for speed control is provided by Simplorer to Simulink through AnsoftSFunction. The FE model of IM is started on no-load with a reference speed of 1440 rpm and is changed to 1300 rpm

at t =1.0 s. The rated load of 40 Nm is applied to the machine at t = 2.0 s. Sinusoidal PWM technique is used to control the inverter with a switching frequency of 2 kHz.

Figure 2 presents the speed of the IM for healthy and single broken bar condition. The ripples in the speed of healthy and faulty IM under steady state can be seen from the enlarged portion and no significant difference is seen except a very slight increase in the speed ripple under faulty condition. The speed control loop acting on the IM tries to keep the average speed in 1300 rpm on both the cases.

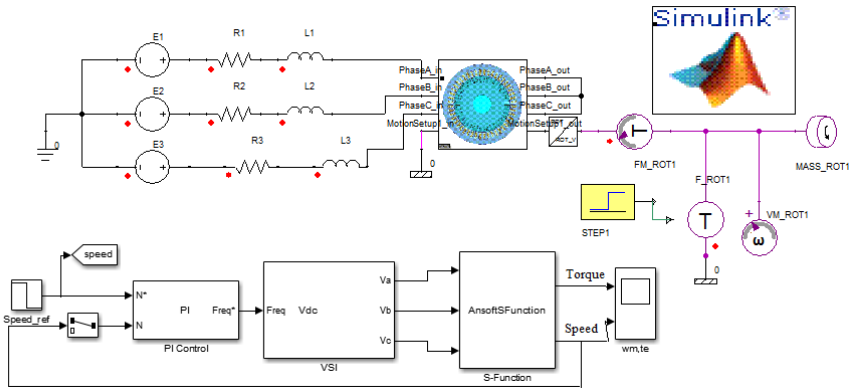

Fig. 1. Block diagram for closed loop *v/f* speed control by co-simulation between ANSYS Maxwell, Simplorer and Matlab Simulink.

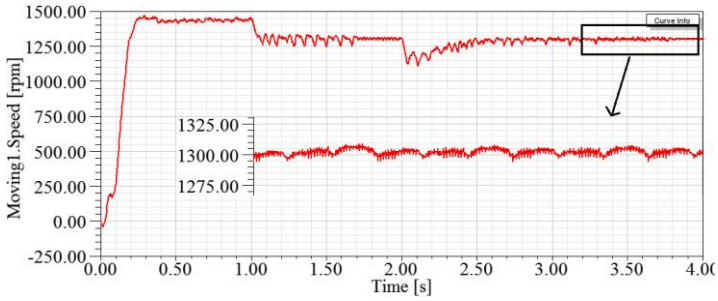

(a) Motor without fault.

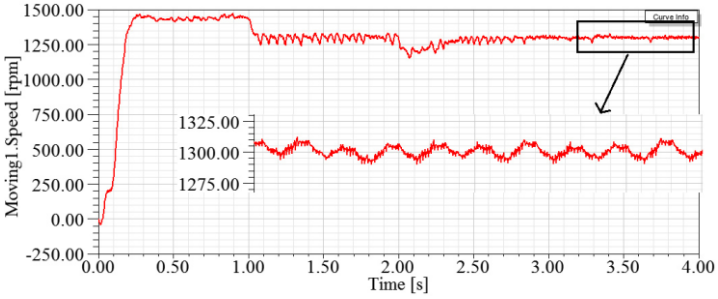

(b) Motor with fault (1 broken bar).

Fig. 2. Speed of IM.

Figure 3(a) displays the flux line distribution of healthy motor, which is symmetric, the magnetic axis of all the poles is located at 90˚ with respect to each other and at any moment of time, the arc of circumference covering all the poles is $\pi D/p$, where D is the stator internal diameter. When a bar gets broken, the magnetic flux distribution becomes asymmetrical due to lack of induced current in the bar broken and increases the current flow to the adjacent bar leading to saturation. Hence, the fault causes a deformation in the magnetic field and produces a deviation in magnetic pole axis as seen in Fig. 3(b). Figure 4 exhibits the distribution of magnetic flux density of IM under healthy and broken bar condition. The deformity in flux distribution near the broken bar leading to saturation in stator and rotor teeth compared to healthy IM is indicated in Fig. 4(b).

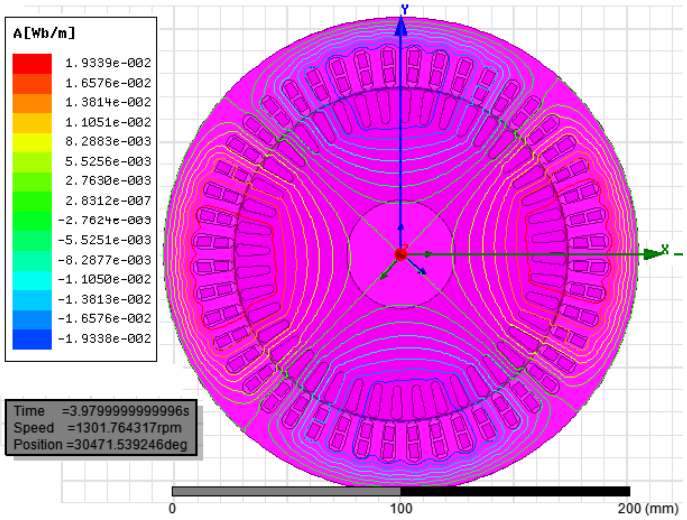

(a) Motor without fault.

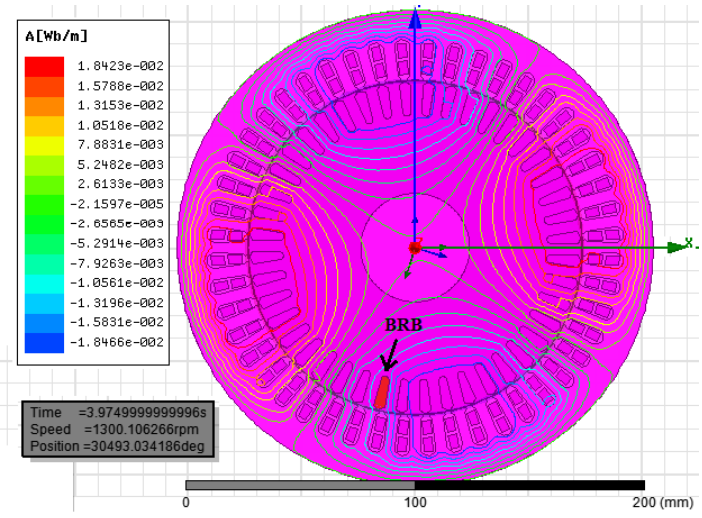

(b) Motor with fault (1 broken bar).

Fig. 3. Circulation of flux lines in IM.

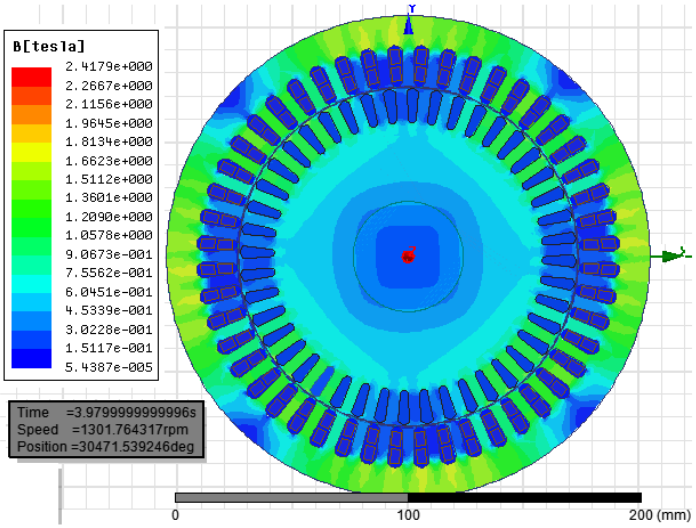

(a) Motor without fault.

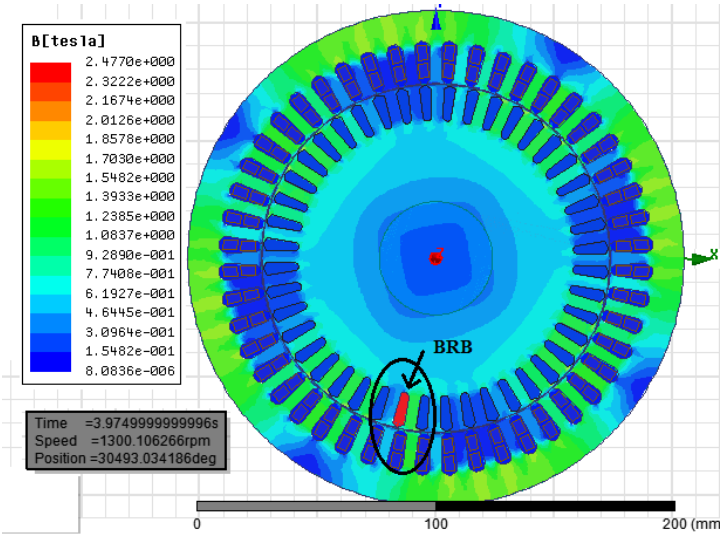

(b) Motor with fault (1 broken bar).

Fig. 4. Distribution of flux density.

4. Radial Airgap Flux Density and Rotor End Connection Analysis

The airgap flux density radial component B_r in cylindrical co-ordinate expressed as an object of B_x and B_y [13], i.e., scalar and vector field,

$$B = \overline{B}.\overline{i_r} = (B_x \overline{i_x} + B_y \overline{i_y}).(Cos[\phi]\overline{i_x} + Sin[\phi]\overline{i_y}) \quad (9)$$

$$\overline{B_r} = B_r \overline{i_r} = B_r (Cos[\phi]\overline{i_x} + Sin[\phi]\overline{i_y}) \quad (10)$$

where φ is the anti-clockwise angle of a stator tooth center with respect to the positive horizontal axis. The airgap flux density radial component of healthy and faulty IM with respect to radial airgap distance at rated load is displayed in Fig. 5. The radial flux density appears like a sinusoid with two electrical cycles for 4-pole machine. The radial airgap field made up of fundamental constituent, stator MMF and rotor MMF harmonics and permeances of stator and rotor slots. The dissymmetry caused by the single broken rotor bar in radial airgap flux density compared to healthy one is indicated in Fig. 5(b). The asymmetry in the magnetic field rises with the austerity of the fault.

Figure 6 depicts the radial airgap flux density spatial FFT spectrum with respect to distance harmonics for healthy and faulty IM at rated load. The healthy motor spectrum Fig. 6(a) shows besides the fundamental constituent of radial airgap flux density with amplitude of around 0.6, the other harmonics, which are having appreciable magnitudes, are around at a distance of 100 mm and 200 mm. When a bar breakage occurs the radial airgap field in addition to fundamental, stator and rotor MMF harmonics will have new harmonic components as noise shown in Fig. 6(b) due to fault. The harmonic noise content will increase with the severity of the fault.

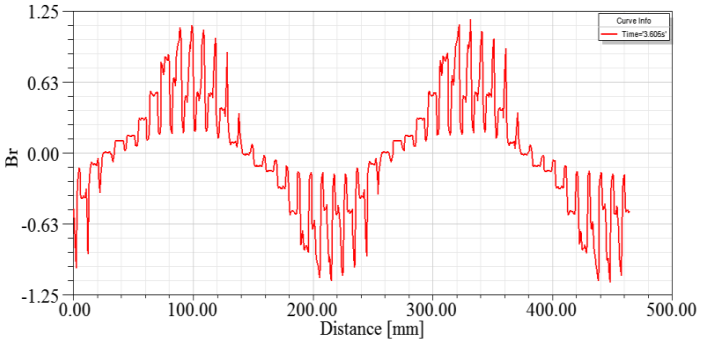

(a) Motor without fault.

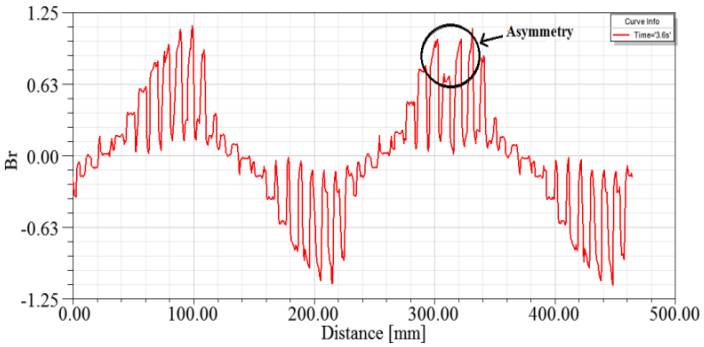

(b) Faulty motor.

Fig. 5. Airgap flux density (radial component).

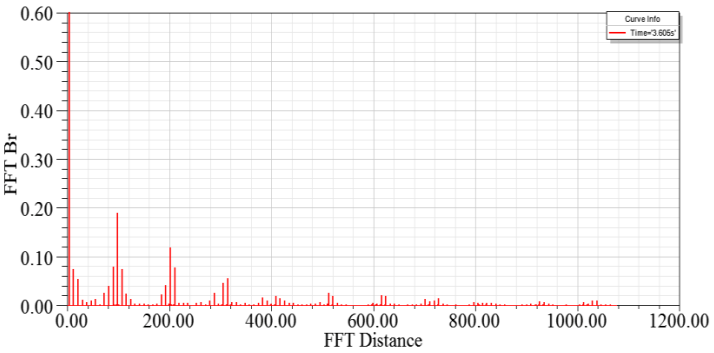

(a) Motor without fault.

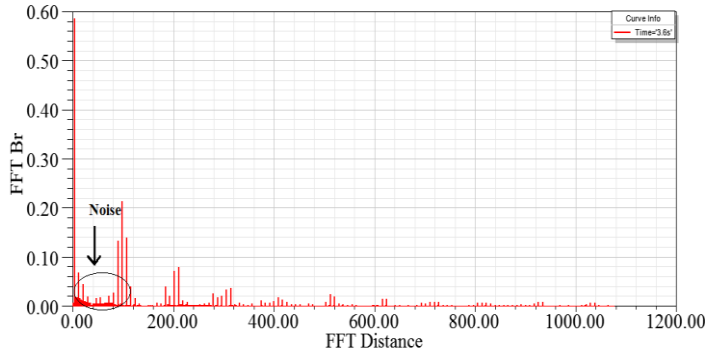

(b) Faulty motor.

Fig. 6. Radial airgap flux density FFT spectrum (spatial).

Figure 7 illustrates the tangential component of airgap flux density under healthy and single broken bar faulty condition and its spatial FFT spectrum is displayed in Fig. 8. The tangential component of flux density is responsible for useful torque in the IM and the radial components are responsible for unnecessary forces, which causes magnetic noise. Hence, the tangential component of airgap flux density has negligible contribution towards magnetic noise, which can be seen from Fig. 8. The tangential FFT spectrum of healthy and faulty motor looks very similar.

In this paper, an attempt is made to analyse the voltage induced in the end connection or end-ring of the rotor under healthy and faulty condition. Figure 9 displays the voltage induced in the end connection of squirrel cage rotor for healthy and faulty IM.

For healthy rotor, the induced voltage at rated load appears to be in the order of millivolts and looks sinusoidal in nature due to balanced operation whereas in the faulty rotor due to lack of induced currents in the broken bar cause an imbalance in the rotor induced voltage and increases its ripple content thereby start losing its sinusoidal nature. The ripple content in the induced voltage of end connection in the faulty rotor increases with the severity of the fault and also its nature can be seen in Fig. 9.

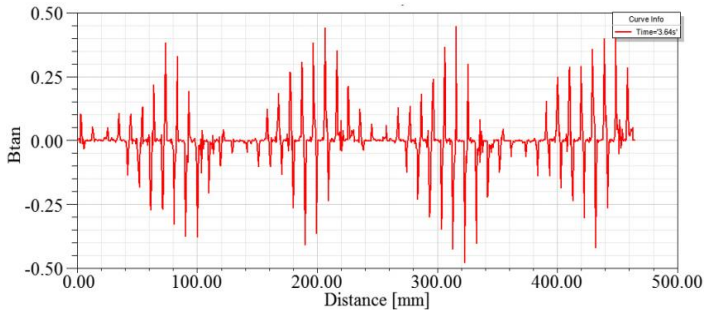

(a) Motor without fault.

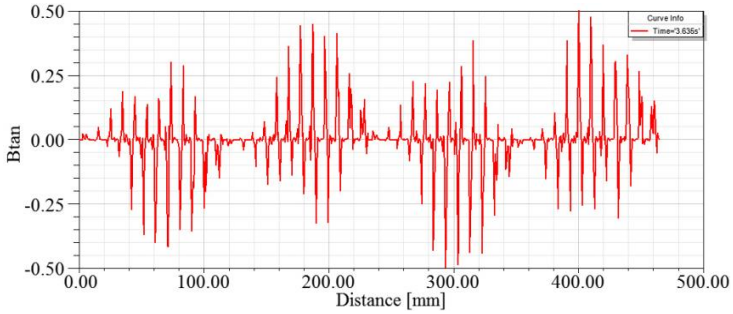

(b) Faulty motor.

Fig. 7. Airgap flux density (Tangential component).

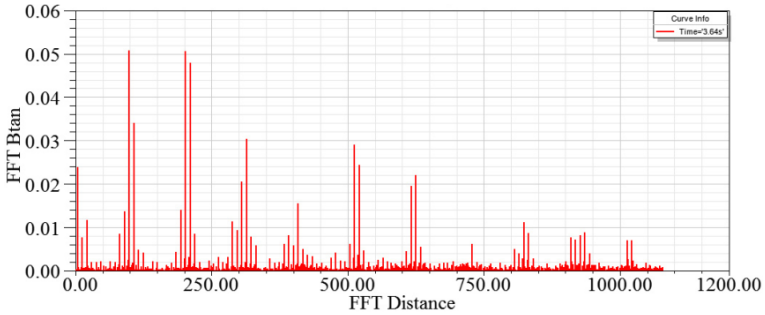

(a) Motor without fault.

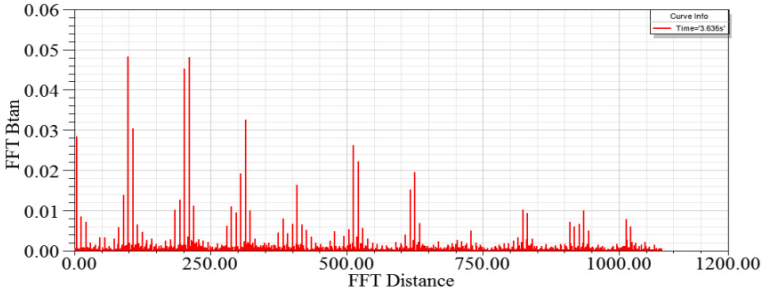

(b) Faulty motor.

Fig. 8. Tangential airgap flux density FFT spectrum (spatial).

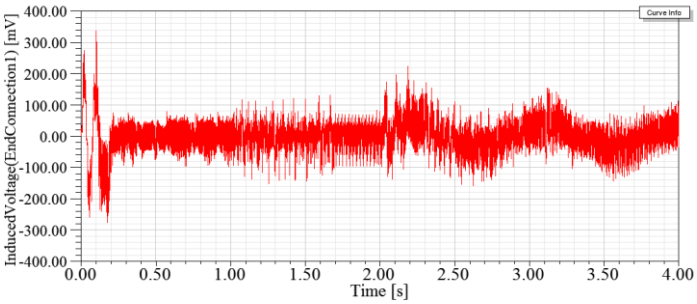

(a) Rotor without fault.

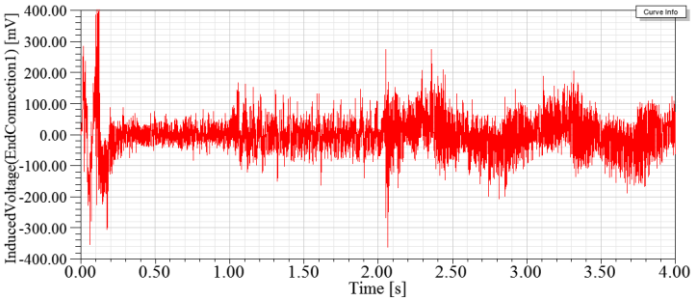

(b) Rotor with fault (1 broken bar).

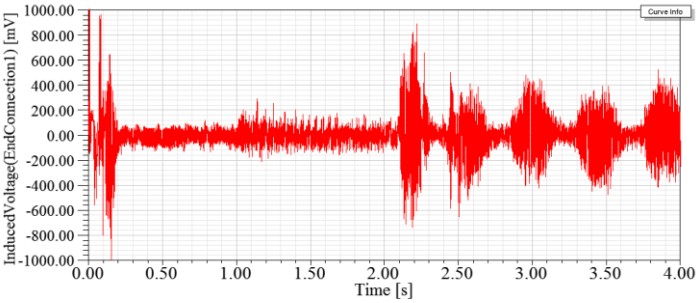

(c) Rotor with fault (2 broken bars).

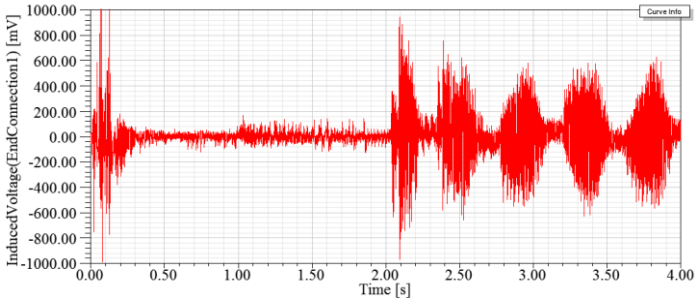

(d) Rotor with fault (3 broken bars).

Fig. 9. Voltage induced in the end-connection of rotor.

5. Conclusions

The electromagnetic field signatures of closed loop speed controlled IM under single broken rotor bar fault were investigated using FEM. Induction motor with a healthy and broken rotor bar model have been created and electromagnetic field parameters are analysed. The radial component of flux density in the airgap of IM is used to analyse the broken bar fault at the incipient stage in a closed loop speed controlled IM. Compared to other fault diagnosis methods where several important aspects like magnetic saturation, spatial harmonics and non-linear behaviour of magnetic materials are neglected and its influence on the findings had certain differences between calculated and practical values, the proposed method includes all the above said aspects in determining the fault at the incipient stage with the help of FEM. In addition, the impact of closed loop technique on the most fault detection algorithm makes it vulnerable to diagnose the fault at the incipient stage.

The results show that the broken rotor bar fault produces a deviation in magnetic pole axis causing dissymmetry in magnetic fields leading to saturation of flux density near the broken bar. The airgap flux density radial component is compared and its spatial FFT spectrum shows in addition to the fundamental, stator MMF and rotor MMF components, new harmonic components as magnetic noise is introduced due to broken rotor bar fault. The noise component in radial airgap flux density increases with the severity of the fault. The tangential component of airgap flux density is accountable for useful torque and hence it has negligible contribution towards the magnetic noise caused by broken bar fault as seen from its FFT spectrum. In addition, an analysis is made on the voltage induced in the end connection of squirrel cage rotor, which was rarely mentioned in the literature, shows an increase in ripple content and deformity of shape based on the severity of number of broken bars.

The future analysis includes the possibility of placing hall effect sensors in the airgap of IM to extract the radial flux density wave for tracing the parameters related to fault. Also radial flux density can be used for analysing and discriminating other faults in IM like stator winding short-circuit fault, eccentricity and bearing fault at the incipient stage.

Nomenclatures

B_r	Radial flux density, Wb/m^2
D	Stator internal diameter, mm
F	Magneto-motive force
K_c	Carter's coefficient
N_s	Stator slot number
N_r	Rotor slot number
P	Number of pole-pairs

Greek Symbols

δ_o	Airgap length, mm
θ	Geometrical angle, deg.
Λ	Permeance
μ	Rotor MMF spatial harmonic
ν	Stator MMF Spatial Harmonic
τ	Spatial half-period of MMF ideal wave

ϕ	Stator tooth center angle with respect to horizontal axis, deg.
φ_μ	Reference angle between stator and rotor fundamental MMF
ω	Angular frequency, rad/s

Abbreviations

DTC	Direct Torque Control
FEA	Finite Element Analysis
FEM	Finite Element Method
FFT	Fast Fourier Transform
FOC	Field Oriented Control
IM	Induction Motor
MMF	Magneto-motive Force
PWM	Pulse Width Modulated
VSI	Voltage Source Inverter

References

1. Filippetti, F.; Bellini, A.; and Capolino, G.-A. (2013). Condition monitoring and diagnosis of rotor faults in induction machines: State of art and future perspectives. *IEEE Workshop on Electrical Machines Design, Control and Diagnosis (WEMDCD)*. Paris, 196-209.
2. Riera-Guasp, M.; Pons-Llinares, J.; Climente-Alarcon, V.; Vedreño-Santos, F.; Pineda-Sánchez, M.; Antonino-Daviu, J.; Puche-Panadero, R.; Perez-Cruz, J.; and Roger-Folch, F. (2013). Diagnosis of induction machines under non-stationary conditions: Concepts and tools. *IEEE Workshop on Electrical Machines Design, Control and Diagnosis (WEMDCD)*. Paris, France, 220-231.
3. Cabanas, M.F.; Pedrayes, F.; Rojas, C.H.; Melero, M.G.; Norniella, J.G.; Orcajo, G.A.; Rodriguez, J.M.C.; Nuno, F.; and Fuentes, D.R. (2011). A new portable, self-powered, and wireless instrument for the early detection of broken rotor bars in induction motors. *IEEE Transactions on Industrial Electronics*, 58(10), 4917-4930.
4. Gyftakis, K.N.; Spyropoulos, D.V.; Kappatou, J.C.; and Mitronikas, E.D. (2013). A novel approach for broken bar fault diagnosis in induction motors through torque monitoring. *IEEE Transactions on Energy Conversion*, 28(2), 267-277.
5. da Silva, A.M.; Povinelli, R.J.; and Demerdash, N.A.O. (2013). Rotor bar fault monitoring method based on analysis of air-gap torques of induction motors. *IEEE Transactions on Industrial Informatics*, 9(4), 2274-2283.
6. Kim, B.; Lee, K.; Yang, J.; Lee, S.B.; Wiedenbrug, E.J.; and Shah, M.R. (2011). Automated detection of rotor faults for inverter-fed induction machines under standstill conditions. *IEEE Transactions on Industry Applications*, 47(1), 55-64.
7. Praveen, K.N.; Isha, T.B.; and Balakrishnan, P. (2016). Radial electro-magnetic field analysis of induction motor under faulty condition using FEM. *Proceedings of the Biennial International Conference on Power and Energy Systems: Towards Sustainable Energy (PESTSE)*. Bangalore, India, 1-6.
8. Praveen K.N.; and Isha, T.B. (2016). Electromagnetic field analysis of 3-Phase induction motor drive under broken rotor bar fault condition using FEM.

Proceedings of the IEEE International Conference on Power Electronics, Drives and Energy Systems (PEDES). Trivandrum, India, 1-6.

9. Bensalem, Y.; and Abdelkrim, M.N. (2016). Modeling and simulation of induction motor based on finite element analysis. *International Journal of Power Electronics and Drive Systems (IJPEDS)*, 7(4), 1100-1109.
10. Godoy, W.F.; da Silva, I.N.; Goedtel, A.; Palácios, R.H.C.; and Lopes, T. D. (2016). Application of intelligent tools to detect and classify broken rotor bars in three-phase induction motors fed by an inverter. *IET Electric Power Applications*, 10(5), 430-439.
11. Zarri, L.; Gritli, Y.; Rossi, C.; Bellini, A.; and Filippetti, F. (2015). Fault detection based on closed-loop signals for induction machines. *Proceedings of the IEEE Workshop on Electrical Machines Design, Control and Diagnosis (WEMDCD)*. Torino, Italy, 261-270.
12. Nemec, M.; Drobnic, K.; Nedeljkovic, D.; Fiser, R.; and Ambrozic, V. (2010). Detection of broken bars in induction motor through the analysis of supply voltage modulation. *IEEE Transactions on Industrial Electronics*, 57(8), 2879-2888.
13. Abu-Elhaija, W.S.; Ghorbanian, V.; Faiz, J.; and Ebrahimi, B.M. (2012). Impact of closed-loop control on behavior of inverter-fed induction motors with rotor broken-bars fault. *Proceedings of the IEEE International Conference on Power Electronics, Drives and Energy Systems (PEDES)*. Bengaluru, India, 1-4.
14. Hou, Z.; Huang, J.; Liu, H.; Ye, M.; Liu, Z.; and Yang, J. (2017). Diagnosis of broken rotor bar fault in open- and closed-loop controlled wye-connected induction motors using zero-sequence voltage. *IET Electric Power Applications*, 11(7), 1214-1223.
15. Hou, Z.; Huang, J.; Liu, H.; Wang, T.; and Zhao, L. (2016). Quantitative broken rotor bar fault detection for closed-loop controlled induction motors. *IET Electric Power Applications*, 10(5), 403-410.
16. Boldea, I.; and Nasar, S.A. (2010). *The induction machines design handbook* (2nd ed.). Boca Raton, Florida: CRC Press.
17. Apostoaia, C.M. (2012). Co-simulation platform for AC drives control systems. *Proceedings of the WASET International Conference on Electric Machines and Drive Systems (ICEMDS)*. Paris, France, 7 pages.